Wireless Power Transfer

cambridge.org/wpt

The effect of rotatory coil misalignment on transfer parameters of inductive power transfer systems

Florian Niedermeier[1,2], Marius Hassler[1,3], Josef Krammer[1] and Benedikt Schmuelling[2]

[1]BMW Group, 80788 Munich, Germany; [2]University of Wuppertal, Rainer-Gruenter-Str. 21, 42119 Wuppertal, Germany and [3]Technical University of Munich, Arcisstr. 21, 80333 Munich, Germany

Research Article

Cite this article: Niedermeier F, Hassler M, Krammer J, Schmuelling B (2019). The effect of rotatory coil misalignment on transfer parameters of inductive power transfer systems. *Wireless Power Transfer* **6**, 77–84. https://doi.org/10.1017/wpt.2019.7

Received: 26 September 2018
Revised: 8 March 2019
Accepted: 18 April 2019
First published online: 7 June 2019

Key words:
Inductive charging; Wireless power transfer; Angular misalignment; Rotatory offset

Author for correspondence:
F. Niedermeier, University of Wuppertal, Rainer-Gruenter-Str. 21, 42119 Wuppertal, Germany. Email: F.Niedermeier@me.com

Abstract

The characteristic transfer parameters of inductive power transfer systems highly depend on the relative position of the coils to each other. While translational offset has been investigated in the past, the effect of rotatory offset on the transfer parameters is widely unclear. This paper contains simulation results of an inductive power transfer system with a rotatory offset in three axes and shows the possible improvements in the coupling coefficient. As a result, rotation angles can be used as control parameters and thereby increase the system efficiency. Alternatively, the allowed misalignment area of the secondary coil can be increased while maintaining the functionality and same dimensions.

1. Introduction

Over the last decade, the research interest in inductive power transfer (IPT) has highly increased due to a wide range of possible applications. In the daily usage of mobile phones, medical implants or electric vehicles (EVs), charging the device is an inevitable task that can benefit from IPT. The contactless charging of EVs comes with many advantages, such as user convenience, insusceptibility to weather and prevention of vandalism [1–9].

The transfer of electrical energy in inductive charging systems is proceeding via an alternating magnetic field between two coils, using the principle of resonant electromagnetic coupling via induction. This way, power can be transferred from the grid to the car through an air gap to charge the battery. Nevertheless, inductive charging results in more complex systems in comparison to conductive charging systems [3, 6, 7]. Using IPT for charging EVs, a major challenge is to design systems that work within a large area of coil positioning, due to parking inaccuracy and various ground clearances. Translatory and rotational misalignment of the coils results in a change of characteristic parameters, so it is important to be able to analyze wireless charging systems in all operating points [10–12]. Only if the characteristic transfer parameters of the electromagnetic coupler are known in all considered misalignments, a simulation of the system including electronic circuitry can be performed.

In this paper, we analyze the behavior of an inductive power transfer system (IPTS) when the secondary coil has a rotational offset toward the primary coil. The effect of rotational misalignment on the characteristic transfer parameters of the IPTS is evaluated and thereby a new optimal position of coils is detected. Using the three rotational angles as additional control parameters, the system can reach new operating points with high magnetic coupling and avoid operating points with low magnetic coupling.

2. Fundamentals

The block diagram in Fig. 1 shows the functional principle of an exemplary IPTS. The most elementary part for IPT is the electromagnetic coupler, which combines two resonant circuits that are galvanically isolated by the air gap. Each resonant circuit consists of an inductor and a capacitor, operating in resonance at a certain frequency f. An inverter processes the DC voltage V_{DC} to get alternating voltage at the input side of the electromagnetic coupler, and the output voltage is rectified to charge the battery with DC voltage. As a result, alternating current resonates in the primary resonant circuit and generates an alternating magnetic field. The magnetic field induces voltage in the secondary side and thereby transfers power through an air gap by means of electromagnetic induction [1, 5, 8, 9, 13–15].

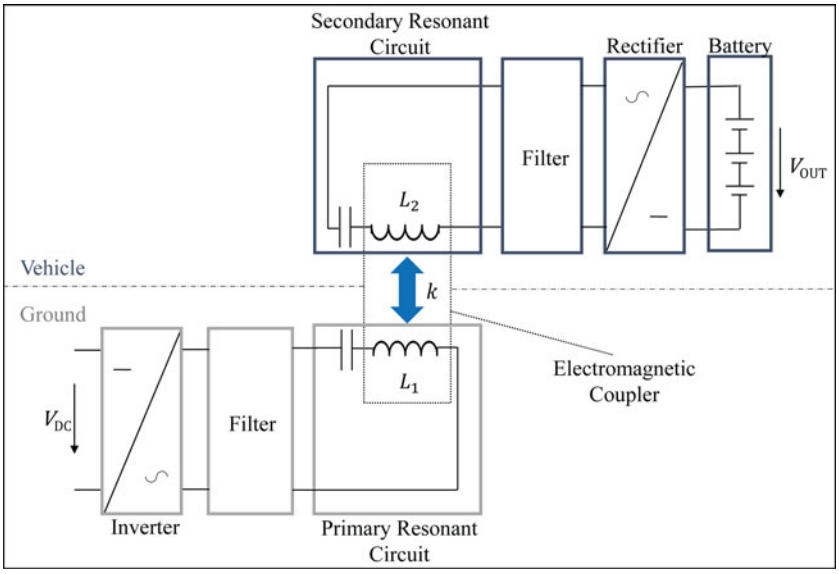

Fig. 1. Block diagram of an exemplary IPTS.

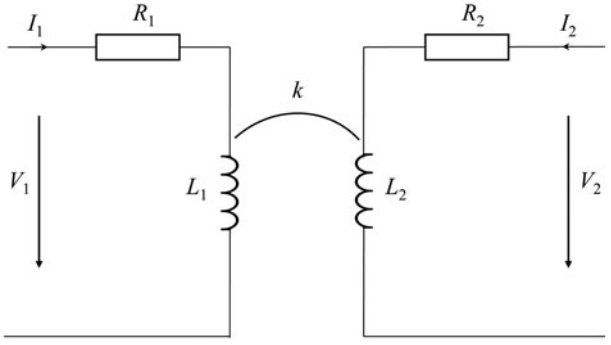

Fig. 2. Equivalent circuit of the electromagnetic coupler.

2.1. Transfer parameters

In a first approach, the electromagnetic coupler can be approximated by a transformer. The difference to a classic transformer is that the leakage inductances are much higher than the mutual inductance because there is an air gap between the coils. The established equivalent circuit of a transformer can be used to describe the electromagnetic coupler with five characteristic transfer parameters: [1, 9, 16, 17]

- mutual coupling k
- primary inductance L_1
- secondary inductance L_2
- primary resistance R_1
- secondary resistance R_2

Figure 2 illustrates that the physical connectedness of the transfer parameters can be described by

$$V_1 = j\omega L_1 I_1 + R_1 I_1 + j\omega M I_2 \quad (1)$$

$$V_2 = j\omega L_2 I_2 + R_2 I_2 + j\omega M I_1 \quad (2)$$

with angular frequency $\omega = 2\pi f$ and mutual inductance $M = k\sqrt{L_1 L_2}$ [9, 18].

The transfer parameters highly depend on the designed geometry of primary and secondary coil, on the electromagnetic properties of materials close to the coupler, and especially on the instantaneous relative position of the coils. The effect of translational misalignment has been widely investigated [3, 19–22]. In this paper, we focus on the investigation of the effect of rotatory misalignment on the transfer parameters.

2.2. Optimization variable: coupling coefficient

The coupling coefficient is defined by the ratio of magnetic flux received in the secondary coil and magnetic flux generated in the primary coil. To ensure that the magnetic flux in the secondary coil is high enough to induce the defined voltage, the principle of electromagnetic resonance is used. Since the primary side is operated in resonance, a high amount of reactive power is resonating between the electric field of the capacitor and the magnetic field of the inductor. This way, the induced secondary voltage is high enough to ensure power transfer, even if the coupling coefficient is low in loosely coupled systems. However, reactive power in real systems is always accompanied by power dissipation due to cable losses and eddy current losses [23].

A high coupling coefficient on the other hand allows to minimize the reactive power in the system, thereby increasing the efficiency of power transfer. The development of an IPTS predominantly requires designing a coil system that offers high coupling coefficients in every allowed operating point with translational or rotatory coil offset. Thus, the coupling coefficient k is one of the most important optimization variables. This can also be seen in the equation for the optimum magnetic transformer efficiency

$$\eta_{opt} = \frac{\chi^2}{\left(1 + \sqrt{1 + \chi^2}\right)^2}, \quad (3)$$

where the figure of merit $\chi = k\sqrt{Q_1 Q_2}$ comprises the coupling coefficient with the quality factors Q_1 and Q_2 of the primary and secondary coil [24].

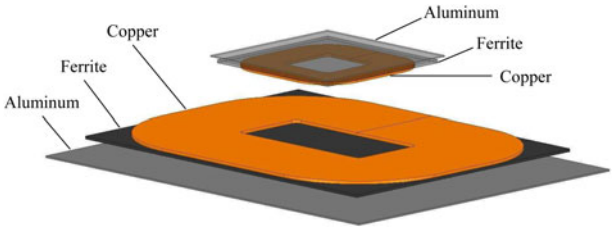

Fig. 3. Simulation model of the electromagnetic coupler.

3. Method

There are two ways to get the transfer parameters of an electromagnetic coupler: measurement and simulation. In this paper, we choose simulation to be able to get the transfer parameters of the system in thousands of positions, for a more significant dataset. The following sections explain the process of modeling and simulation.

3.1. Simulation with finite element method

A number of pertinent software applications are capable of calculating the required values by means of the finite element method (FEM). For this project, *ANSYS Maxwell*, a high-performance software package that uses FEM to solve electromagnetic field problems, is chosen. By solving the Maxwell equations

$$\nabla \times \vec{E} = -\frac{\partial \vec{B}}{\partial t} \quad ; \quad \nabla \cdot \vec{D} = \rho \tag{4}$$

$$\nabla \times \vec{H} = \vec{J} + \frac{\partial \vec{D}}{\partial t} \quad ; \quad \nabla \cdot \vec{B} = 0 \tag{5}$$

in a finite region with boundary conditions, *ANSYS Maxwell* can obtain a unique solution of electromagnetic field problems of various kinds. The finite elements are defined as tetrahedrons and the field in each element is approximated with a quadratic polynomial of second order. All values are put together to one large, sparse matrix equation that is solved by applying the Sparse Gaussian Elimination. This way, the elementary transfer parameters k, L_1, and L_2 of diverse electromagnetic couplers can be calculated via simulation with high accuracy.

3.2. Modeling

In this paper, we investigate the effect of rotation and tilt of the secondary module on the transfer parameters. Therefore, we use the circular coil system that is proposed by the *Society of Automotive Engineers* (*SAE*) in its Information Report of standard *SAE J2954* [25]. The geometric modeling of the coil system can be restricted to materials that influence electromagnetic fields, so the created model only consists of aluminum, copper, and ferrite. Additional material (i.e. plastic, air, filling material) is not significant for this investigation. To reduce complexity, two simplifications are made: the ferrite tiles are modeled as one solid ferrite plate, and the windings are approximated by one solid ring with homogeneous current density. The whole model can be seen in Fig. 3, illustrating two coils, two ferrite cores and two shielding plates.

The transfer parameters of an electromagnetic coupler highly depend on the instantaneous relative position of the coils. The *SAE J2954* considers a mutual coil offset of $-75\ \text{mm} \leq x \leq 75\ \text{mm}$ in driving direction and $-100\ \text{mm} \leq y \leq 100\ \text{mm}$ in the transverse direction. For vertical displacement, it defines several z-classes specified by the respective ground clearances. The class z_1 is defined by a ground clearance range of $100\ \text{mm} \leq z_{gc} \leq 150\ \text{mm}$. Based on these data, the secondary coil is misaligned in x- and y-direction in the range of

$$-80\ \text{mm} \leq x \leq 80\ \text{mm} \tag{6}$$

$$-120\ \text{mm} \leq y \leq 120\ \text{mm} \tag{7}$$

with steps of 20 mm in both directions while the primary coil is fixed. The vertical distance of primary and secondary coil is set to a fixed coil-to-coil distance of $z_{c2c} = 75\ \text{mm}$, which corresponds roughly to the center of class z_1.

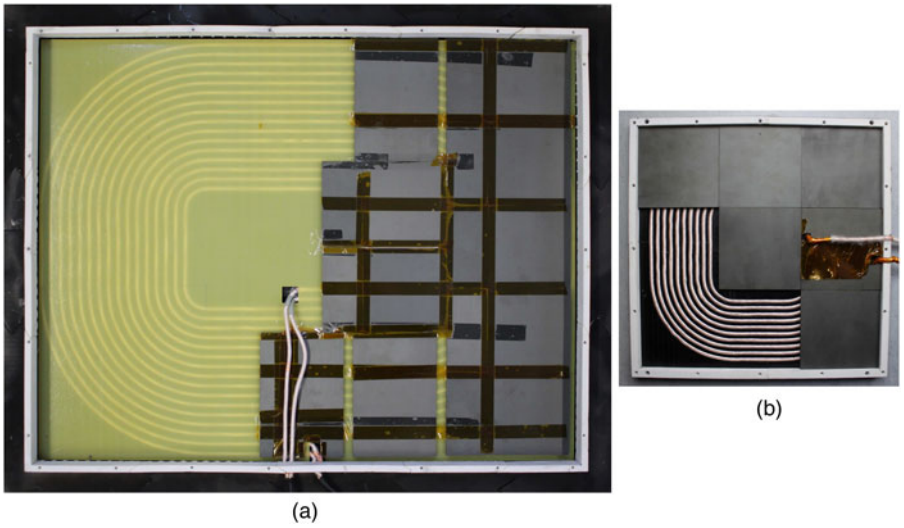

Fig. 4. Photograph of the measuring object. (a) Primary coil. (b) Secondary coil.

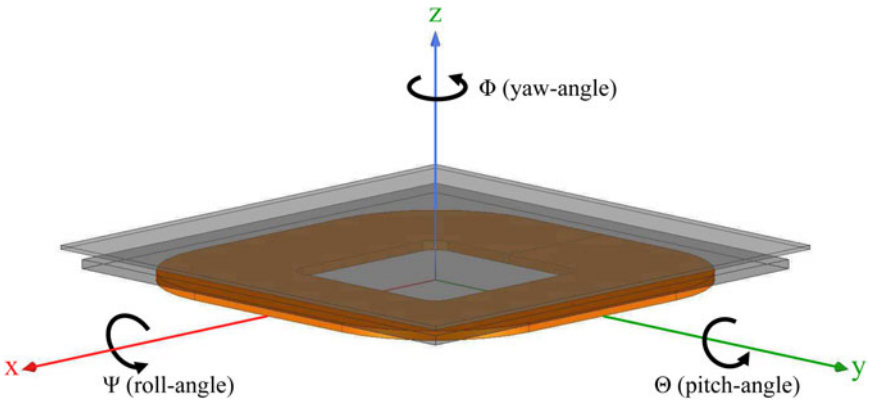

Fig. 5. Three angles of rotation in relation to the secondary coil.

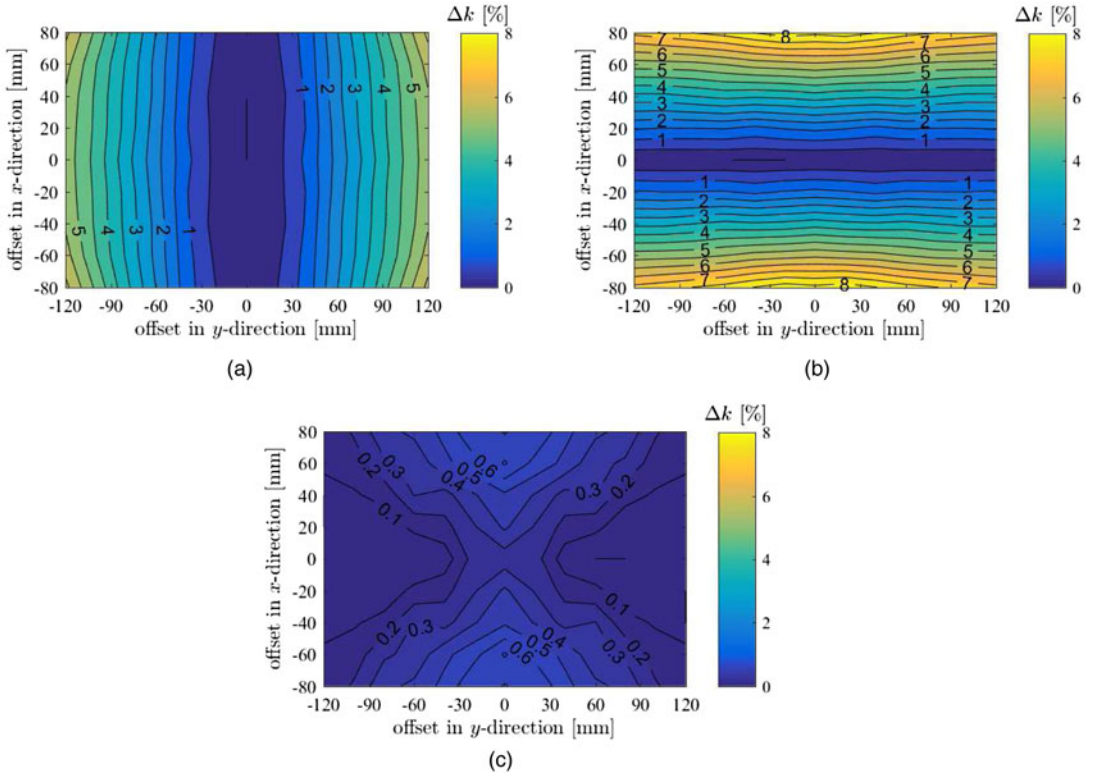

Fig. 6. Improvement of coupling coefficient Δk for mono-axial rotation. (a) Rotation in Ψ (around x-axis). (b) Rotation in Θ (around y-axis). (c) Rotation in Φ (around z-axis).

3.3. Measurements

A coil system has been built in accordance with the standard *SAE J2954* to verify the simulations and the modeling method. The coil system is able to transfer up to 3.6 kW over the lateral displacement range defined in equations (6) and (7). Figure 4 shows pictures of the manufactured primary and secondary device.

For measuring the transfer parameters, low-power measurements are conducted. A total of 7626 positions have been measured, equally distributed over the misalignment area depicted above. The coupling coefficient of every position is compared to the respective simulated value and the results show that the simulated coupling coefficient differs from the measured coupling coefficient only by 2.65% on average. These results verify that the presented modeling method can be applied for further simulation and that the simulation results can serve as a verified base for drawing further conclusions.

3.4. Rotation and tilting of the secondary coil

Apart from translational misalignment, the coil system can also have a rotatory offset. To investigate the effect of rotatory offset, the secondary coil can be rotated in three axes: longitudinal x-axis (roll-angle: Ψ), lateral box$y$-axis (pitch-angle: Θ), and vertical z-axis (yaw-angle: Φ) [25]. Figure 5 illustrates the three axes and the rotating direction. In this case, the origin of the coordinate system is set to the middle of the secondary coil, on the bottom of the copper.

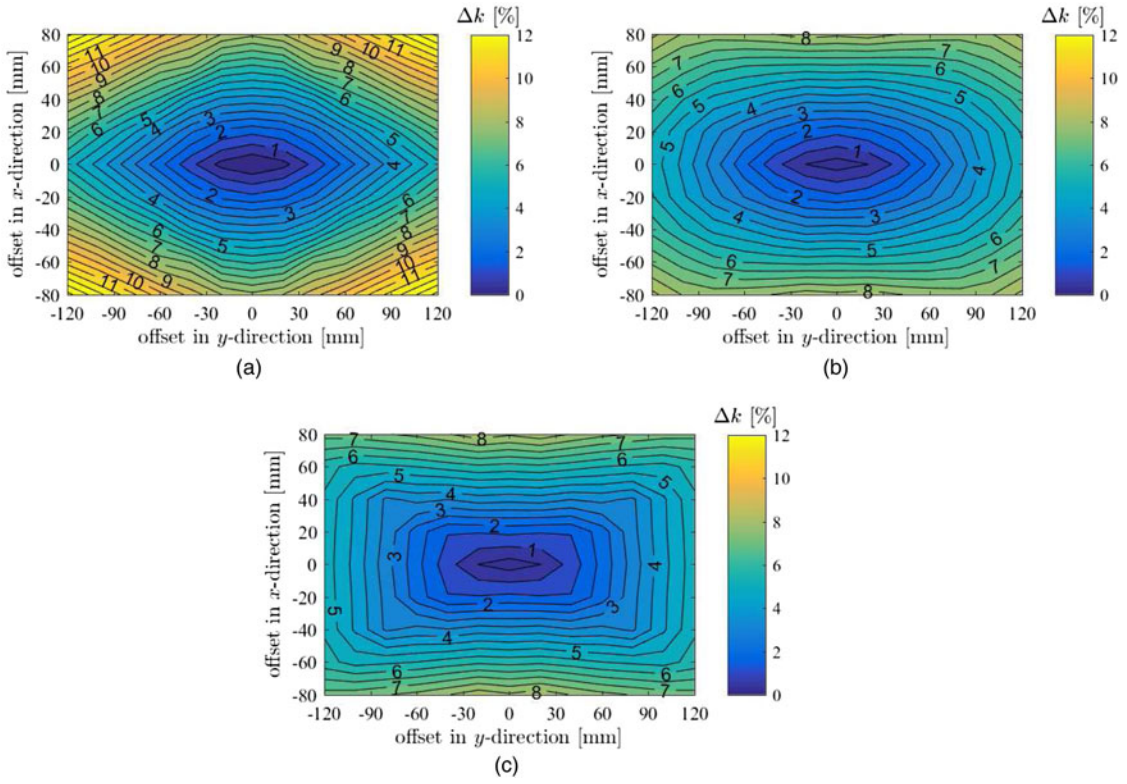

Fig. 7. Improvement of coupling coefficient Δk for bi-axial rotation. (a) Rotation in Ψ and Θ (around x, y-axes). (b) Rotation in Θ and Φ (around y, z-axes). (c) Rotation in Ψ and Φ (around x, z-axes).

To get a representative dataset, the coil system is simulated for

$$-6^\circ \leq \Psi \leq 6^\circ$$
$$-6^\circ \leq \Theta \leq 6^\circ$$
$$0^\circ \leq \Phi \leq 90^\circ$$

with steps of 2° in Ψ and Θ, and with steps of 15° in Φ. The range of $-90^\circ \leq \Phi < 0^\circ$ is redundant due to symmetries when the secondary coil is rotating. Summing up all translational and rotatory misalignments, the coil system is simulated in 40131 different positions.

Table 1. Overview of maximum change in transfer parameters.

Rotation angle	Δk^{max}	$\overline{\Delta k}$	ΔL_1^{max}	ΔL_2^{max}
Ψ	6.1%	2.5%	1.5%	0.3%
Θ	8.3%	3.7%	1.2%	0.3%
Φ	0.7%	0.3%	0.7%	0.2%
$\Psi + \Theta$	13.2%	6.1%	2.6%	0.5%
$\Theta + \Phi$	8.6%	4.5%	1.9%	0.4%
$\Psi + \Phi$	8.3%	4.9%	1.8%	0.3%
$\Psi + \Theta + \Phi$	13.2%	6.9%	3.1%	0.5%

4. Results and discussion

Due to better visualization of differences that come along with rotation, the results are described as improvement potential Δk, which is defined as the percentage change of the coupling coefficient with respect to the zero-rotation value. At each allowed offset position, the secondary coil is rotated within its rotational range as stated in the previous section. First, the rotation along a single axis is studied to see the effects of each rotation direction individually. Then, the results for combinations of different rotation directions are given.

4.1. Rotation around one axis

Figure 6 shows the maximum possible improvement in the coupling coefficient that can be achieved at each position for rotation around one single axis. Figure 4 illustrates that a rotation around the x-axis

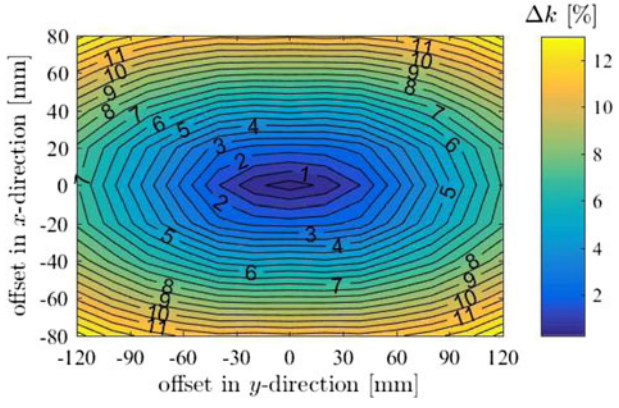

Fig. 8. Improvement of coupling coefficient Δk for tri-axial rotation.

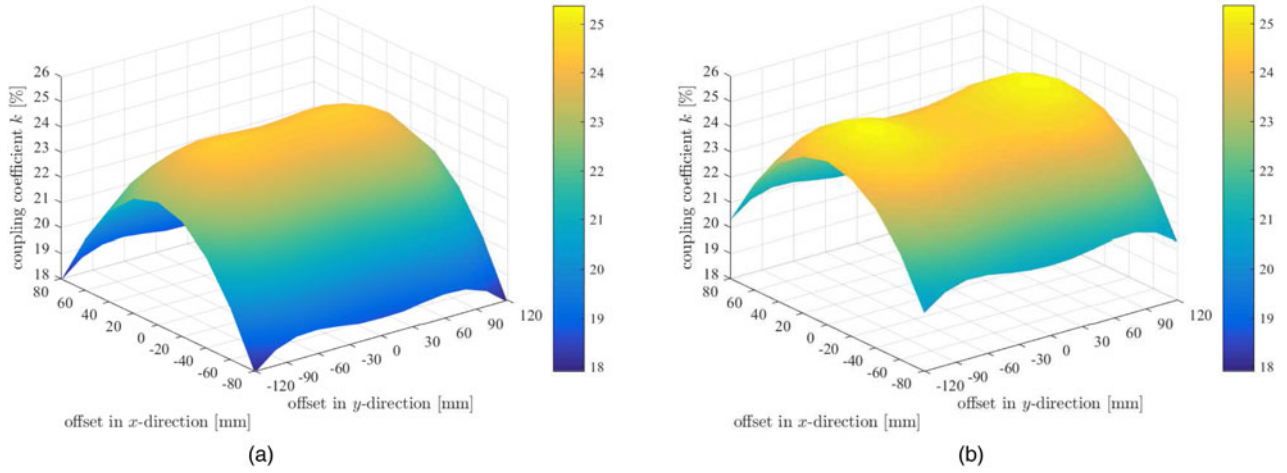

Fig. 9. Comparison of absolute values of coupling coefficient k. (a) Without rotation. (b) With bi-axial rotation.

can improve the coupling coefficient up to $\Delta k_{\Psi}^{\max} = 6.1\,\%$. The mean value taken over all positions reveals an increase in coupling coefficient of $\overline{\Delta k_{\Psi}} = 2.5\,\%$. A rotation around the y-axis yields the highest improvement for mono-axial rotation. The maximum increase is given by $\Delta k_{\Theta}^{\max} = 8.3\,\%$ (see Fig. 4). In addition to the highest improvement, it also achieves the highest mean value with an increase of $\overline{\Delta k_{\Psi}} = 3.7\,\%$. Figure 4 shows that a single rotation around the z-axis can be neglected as it merely results in changes below 1%. The increase in coupling coefficient can be understood by consideration of the magnetic flux. The current inside the primary coil generates magnetic field lines, which have more horizontal components at a higher offset from the origin. As only the field lines perpendicular to the receiving coil induce voltage, rotation can increase the coupling coefficient. The perpendicular flux through the receiving coil can be maximized at the outer positions in particular. The magnetic field in x-direction B_x increases with x-offset from the origin. Therefore, a rotation around the y-axis can increase the coupling coefficient. Analogously, at positions with y-offset the coupling coefficient can be maximized by rotating the secondary coil around the x-axis.

4.2. Rotation around two axes

The effect of rotating the receiving coil around two axes on the coupling coefficient of the system is depicted in Fig. 7. The benefits of mono-axial rotation can be combined to further exceed the improvements. Especially rotating around x- and y-axis can yield significant improvements. The highest improvement rates with $\Delta k_{\Psi\Theta}^{\max} = 13.2\,\%$ can be obtained for the outer offset positions. With an offset in x- and y-direction, the magnetic field components B_x and B_y raise. These components can only be utilized to raise the induced voltage when the receiving coil is tilted in both directions. The mean value over the whole offset range of Fig. 7(a) calculates to $\overline{\Delta k_{\Psi\Theta}} = 6.1\,\%$. A combination with z-axis rotation (see Figs 7(b) and 7(c)) severely influences the profile of the coupling coefficient x-offset for Ψ, Φ-rotation, and y-offset for Θ, Φ-rotation, but cannot support to reach higher maximum values. Table 1 gives a comprehensive overview of the maximum and mean values for the different rotation angles, including the respective inductances. Note: when considering also $-90° \leq \Phi \leq 0°$ (Figs 7(b) and 7(c)) become essentially identical.

4.3. Rotation around three axes

Figure 8 illustrates the improvement of the coupling coefficient that can be achieved for a receiving coil with a full rotational degree of freedom. Thereby, a maximum improvement of up to $\Delta k_{\Psi\Theta\Phi}^{\max} = 13.2\,\%$ can be achieved. The coupling coefficient can be increased at all positions. This is also represented in the mean value, which is raised to $\overline{\Delta k_{\Psi\Theta\Phi}} = 6.9\,\%$. For positions with high offset in x- and y-direction, the coupling coefficient can be raised with increasing yaw-angle until it reaches a maximum at $|\Phi| = 45°$. Therewith, Φ-rotation can improve the coupling coefficient with up to 3%.

4.4. Discussion

A summary of possible improvements of the coupling coefficient for different rotations in the studied offset range is given in Table 1. The highest percentage improvement can be realized when rotation around all axes is used. However, the results show that also the combined rotation around x- and y-axis is similarly potent. The study shows that the introduction of two new control parameters, roll-angle Ψ and pitch-angle Θ, can improve the coupling coefficient and therewith the system efficiency. High improvement rates of up to 13.2 % can be achieved in particular at the outer offset positions, where low coupling coefficients prevail. In Fig. 9, the absolute coupling values are compared. Figure 9(a) shows the coupling coefficient values without rotation. In Fig. 9(b), the maximum coupling coefficient for all bi-axial rotations is depicted. It clearly shows that the absolute values are raised at all positions. In addition, it also shows that the position of the maximum values changes. Without rotation, the maximum position is at $(x, y) = (0, \pm 60)$ mm while the maximum position for the system with full rotational freedom shifts to $(x, y) = (0, \pm 80)$ mm. The control parameters for the new optimum are

$$\Psi = 6^{\circ} \text{ and} \tag{8}$$

$$\Theta = 0^{\circ}\,. \tag{9}$$

Another advantage that comes with the introduction of the new control parameters Ψ and Θ is the extension of the working offset

positions. The offset range is coupled to the lowest coupling coefficient, which is generally defined by maximum offset in all directions. The minimum of the coupling coefficient hence defines the possible offset range. Considering the *SAE J2954* offset range and vertical coil distance $z_{c2c} = 75$ mm, the minimum coupling coefficient of the system without rotation is $k_{\min} = 19.2\,\%$ at $(x, y) = (\pm 75, \pm 100)$ mm. This offset range can be extended to $(x, y) = (\pm 90, \pm 120)$ mm with the new control parameters. The applied angles of rotation are $\Psi = \Theta = \pm 6°$. This way, the allowed offset range can be increased by 44 % while maintaining the functionality and same dimensions. Alternatively, this also allows to decrease the coil size while retaining the same functional offset range.

If it is not possible to set the rotation angles as control parameters but they come as random parameters, the rotatory offset can also negatively affect k. In the worst case for the considered operating area, the coupling coefficient even decreases up to $\Delta k^{wc}_{\Psi\Theta\Phi} = -14.7\,\%$ at $(x, y) = (\pm 80, \pm 120)$. There, the coil is rotated by $\Psi = \Theta = \pm 6°$ into the opposite direction than for optimal improvement shown in the previous section. This rotation decreases the coupling coefficient, as the perpendicular flux through the receiving coil is reduced.

5. Conclusion

In this study, we use FEM simulation to evaluate the effects of rotatory coil misalignment on transfer parameters of IPTS. The results show that the coupling coefficient can be increased with each rotation axis. Highest changes in coupling coefficient can be achieved for the combination of all rotation axes. Rotation around x- and y-axis already achieves high improvements, whereas additional z-axis rotation further improves only slightly. This finding can be easily applied in EVs with air suspensions for stationary charging. The height of the air suspensions can be set individually to match the best coupling coefficient for efficient power transfer in this position. This way, two new control parameters can be utilized to extend the system performance.

References

[1] **Zahid Z, Dalala Z and Zheng C** (2014) Modeling and control of series-series compensated inductive power transfer system. *IEEE J. Emerging Sel. Topics Power Electron.* **3**, 111–123.

[2] **Raju S, Wu R and Chan M** (2014) Modeling of mutual coupling between planar inductors in wireless power applications. *IEEE Trans. Power Electron.* **29**, 481–490.

[3] **Niedermeier F, Krammer J and Schmuelling B** (2016) A Linear Regression Based Method for Estimating Magnetic Parameters of Inductive Power Transfer Systems, IEEE PELS Workshop on Emerging Technologies: Wireless Power, Knoxville (USA).

[4] **Imura T and Hori Y** (2011) Maximizing Air Gap and efficiency of magnetic resonant coupling for wireless power transfer using equivalent circuit and Neumann formula. *IEEE Trans. Ind. Electron.* **58**, 4746–4752.

[5] **Kim J, Kong S and Kim H** (2013) Coil design and shielding methods for a magnetic resonant wireless power transfer system. *Proc. of the IEEE* **101**, 1332–1342.

[6] **Wu H, Gilchrist A and Sealy K** (2012) A high efficiency 5 kW inductive charger for EVs using dual Side control. *IEEE Trans. Ind. Inf.* **8**, 585–595.

[7] **Budhia M, Covic G and Boys J** (2011) Design and optimization of circular magnetic structures for lumped inductive power transfer systems. *IEEE Trans. Power Electron.* **26**, 3096–3108.

[8] **Covic G and Boys J** (2013) Inductive power transfer. *Proc. IEEE* **101**, 1276–1289.

[9] **Wang C, Stielau O and Covic G** (2005) Design considerations for a contactless electric vehicle battery charger. *IEEE Trans. Ind. Electron.* **52**, 1308–1314.

[10] **Fotopoulou K and Flynn B** (2011) Wireless power transfer in loosely coupled links. *IEEE Trans. Magn.* **47**, 416–430.

[11] **Pinuela M, Yates D, Lucyszyn S and Mitcheson P** (2013) Maximizing DC-to-load efficiency for inductive power transfer. *IEEE Trans. Power Electron.* **28**, 2437–2447.

[12] **Sample A, Meyer D and Smith J** (2011) Analysis, experimental results, and range adaptation of magnetically coupled resonators for wireless power transfer. *IEEE Trans. Ind. Electron.* **58**, 544–554.

[13] **Mur-Miranda J and Fanti G** (2010) Wireless Power Transfer Using Weakly Coupled Magnetostatic Resonators, IEEE Energy Conversion Congress and Exhibition (ECCE), Atlanta (USA).

[14] **Mou X and Sun H** (2015) Wireless Power Transfer: Survey and Roadmap, IEEE Vehicular Technology Conference (VTC), Boston (USA).

[15] **Niedermeier F, Hassler M, Krammer J and Schmuelling B** (2017) A Jacobi Based Method for Calculating the Steady State Characteristics of Non-Linear Circuit Elements, IEEE Vehicular Power and Propulsion Conference (VPPC), Belfort (France).

[16] **Jiwariyavej V, Imura T and Hori Y** (2015) Coupling coefficients estimation of wireless power transfer system via magnetic resonance coupling using information from either Side of the system. *IEEE J. Emerging Sel. Topics Power Electron.* **3**, 191–200.

[17] **Schuylenbergh K and Puers R** (2009) *Inductive Powering – Basic Theory and Application to Biomedical Systems*. Dordrecht, Netherlands: Springer.

[18] **Zhang W, Wong S and Tse C** (2014) Design for efficiency optimization and voltage controllability of series compensated inductive power transfer systems. *IEEE Trans. Power Electron.* **29**, 191–200.

[19] **Dang Z and Abu Qahouq J** (2015) Elimination method for the Transmission Efficiency Valley of Death in laterally misaligned wireless power transfer systems, IEEE Applied Power Electronics Conference (APEC), Charlotte (USA).

[20] **Kurschner D, Rathge C and Jumar U** (2013) Design methodology for high efficient inductive power transfer systems with high coil positioning flexibility. *IEEE Trans. Ind. Electron.* **60**, 372–381.

[21] **Zhang W, White J, Abraham A and Mi C** (2015) Loosely coupled transformer structure and interoperability study for EV wireless charging systems. *IEEE Trans. Power Electron.* **30**, 6356–6367.

[22] **Liu F, Yang Y, Jiang D, Ruan X and Chen X** (2017) Modeling and optimization of magnetically coupled resonant wireless power transfer system with varying spatial scales. *IEEE Trans. Power Electron.* **32**, 3240–3250.

[23] **Abdolkhani A** (2016) Fundamentals of inductively coupled wireless power transfer systems. In Coca E (ed.), *Wireless Power Transfer – Fundamentals and Technologies*. Rjieka, Croatia: InTech.

[24] **Vandevoorde G and Puers R** (2001) Wireless energy transfer for stand-alone systems. *Sens. Actuators A* **92**, 305–311.

[25] **J2954 TIR - Wireless Power Transfer for Light-Duty Plug-In/ Electric Vehicles and Alignment Methodology** (2016) SAE International. https://doi.org/10.4271/J2954_201605.

Florian Niedermeier received his B.Sc. degree in electrical engineering from the Technical University of Vienna, Austria, and his M.Sc. degree in electrical engineering from the Technical University of Munich, Germany. He is currently working on his Dr.-Ing. degree at the University of Wuppertal, Germany, and works as a research associate at BMW Group. His main research interests are simulation and analysis of inductive power transfer systems.

Marius Hassler received his B.Sc. and M.Sc. degree in physics with specialization in condensed matter from the Technical University of Munich, Germany. He is currently working toward the Dr.-Ing. degree in engineering with BMW Group, from the Technical University of Munich, Germany. His current research interests include circuit simulation and inductive charging.

Josef Krammer received the Dipl.-Ing. degree in electrical engineering from the Department of Electrical and Computer Engineering at the Technical University of Munich, TUM, Germany. He worked as a researcher at the Institute of Circuit Theory and Signal Processing at the TUM where he received the degree of Dr.-Ing. Since 1991 he is working at BMW Group in different engineering positions for the development of electronics for conventional and electric vehicles.

Benedikt Schmuelling received the M.Sc. degree (Dipl.-Ing.) in electrical engineering from the Faculty of Electrical Engineering and Information Technology of Dortmund University, Germany, in 2005. From 2005 until 2010, he worked as a researcher at the Institute of Electrical Machines, RWTH Aachen University, Germany, where he also received his Ph.D. degree in 2009. From 2010 until 2012, he was with Vahle Inc., Kamen, Germany, where he worked as an engineer on the development of wireless charging stations for electric vehicles. Since 2012 he is with the University of Wuppertal, Germany, where he is the head of the Chair of Electric Mobility and Energy Storage Systems at the School of Electrical, Information and Media Engineering. His research fields include electric mobility, wireless power transfer, renewable energies, energy storage systems, and efficiency topics.